Non-thermal X-rays from pulsation-driven shocks in Cepheids

Federico Fraschetti,[a,b,*] **Konstantina Anastasopoulou,**[a] **Jeremy J. Drake**[a] **and Nancy R. Evans**[a]

[a]*Center for Astrophysics | Harvard & Smithsonian, 60 Garden Street, Cambridge MA 02138, USA*

[b]*Department of Planetary Sciences - Lunar and Planetary Lab, Tucson, AZ, 85721*

E-mail: federico.fraschetti@cfa.harvard.edu

The association of Cepheid pulsation with traveling shocks and therefore X-ray non-thermal emission has been postulated for decades. Here we report the possibly first evidence of shock-accelerated GeV electrons emitted at the archetype classical Cepheid star δ-Cep observed by XMM-Newton and Chandra. We jointly analyse the XMM-Newton thermal and non-thermal components of the time-resolved X-ray spectra prior to, during and after an X-ray enhancement. A comparison of the time scales of the diffusive particle acceleration at shocks with energy loss time scales is consistent with the scenario of a pulsation-driven shock wave traveling into the stellar corona and accelerating electrons to ~GeV energies and with Inverse Compton (IC) emission from the UV stellar background leading to the observed X-ray enhancement. The index of the non-thermal IC photon spectrum, assumed to be a simple power-law in the [1-8] keV energy range, radially integrated within the shell [3 - 10] stellar radii, is consistent with an enhanced X-ray spectrum powered by shock-accelerated electrons. A 100-fold amplification of the magnetic field via turbulent dynamo at the shock propagating through density inhomogeneities in the stellar corona would be required for the synchrotron emission to dominate over the IC; however, such amplification is unlikely for the expected low Mach number shock produced. The lack of time-correlation between radio synchrotron and stellar pulsation contributes to make synchrotron emission as an unlikely mechanism for the flux enhancement. Current observations cannot rule out a high-flux two-temperature thermal spectrum with a negligible non-thermal component.

*Speaker

1. Introduction

The evidence of non-thermal X-ray emission from pulsation-driven shocks at Cepheids has been uncertain for decades. We have analyzed *XMM-Newton* observations of a 4-fold enhancement of the $(0.3 - 2.5)$ keV X-ray flux from the archetype Cepheid δ Cep [1]. Soft X-ray emission from gas heated by radiation-driven shock waves travelling into the gas at the base of stellar wind was modeled by [2]. This mechanism was revised to interpret the hard X-ray [3] and γ-ray emissions [4] from OB supergiants as Inverse Compton (IC) emission from the UV field photons upscattered by the shock-accelerated electrons.

Here we outline our recent analysis [5] of the thermal and possible non-thermal components of the X-ray spectrum of δ Cep during the flux enhancements observed by *XMM-Newton* and Chandra [1]. We have compared acceleration and energy loss time scales for electrons accelerated at the pulsation-driven shocks to identify plausible mechanisms of non-thermal emission. We find that the time scale of IC scattering of the UV photons from the stellar radiation field off the shock-accelerated electrons could give rise to rapid non-thermal flux increases.

2. Analysis of X-rays observations

We have performed a new analysis of the *XMM-Newton* data [1], combining a thermal and a power-law spectral model. We fitted separately the high-flux ($f_{0.3-2.5\,\text{keV}} > 8 \times 10^{-15}\,\text{erg}\,\text{s}^{-1}\,\text{cm}^{-2}$) and the low-flux ($f_{0.3-2.5\,\text{keV}} < 8 \times 10^{-15}\,\text{erg}\,\text{s}^{-1}\,\text{cm}^{-2}$) observations.

For a one-temperature thermal spectral model, the X-ray flux above ~ 1 keV is significantly greater than the thermal flux and the spectrum can be fitted with a single power law in the range $[1 - 8]$ keV; details on the observation IDs and the exposure times can be found in [5].
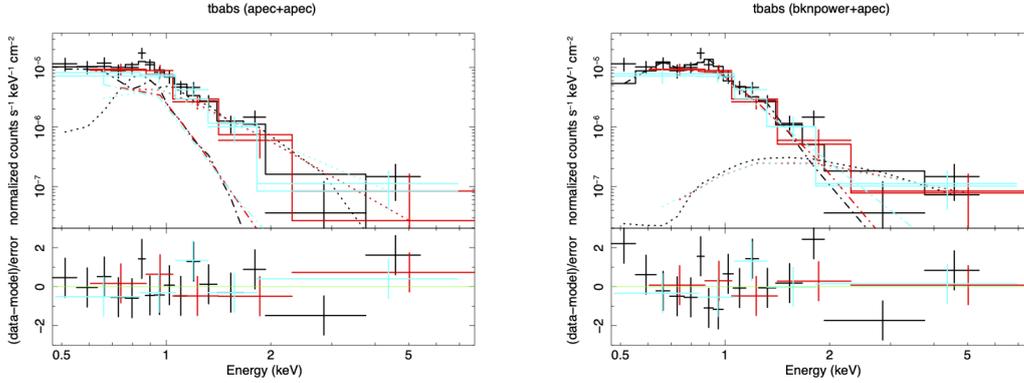
Figure 1: Fit of all EPIC detectors (pn:black, MOS1:red, and MOS2:cyan) for the high-flux observation of δ Cepheid. Left: integrated X-ray spectrum, along with the best-fit model of two absorbed APEC components (dashed-dotted line and dotted line, respectively) in the top panel, and fit residuals in terms of sigmas with error bars of size 1σ in the bottom panel. Right: same as left with the best-fit model of an absorbed APEC component (dash-dotted line) and a power-law component (dotted line).

High-flux spectrum. In order to explore the contribution of a possible non-thermal component at higher energies (>1.5 keV) we introduced a "broken power law" model (model in XSPEC:

`tbabs×(bknpower+apec)`) where the power-law photon index Γ above a certain energy break E_0 is positive (declining spectrum at large energy). The energy break and the power-law photon index Γ for $E > E_0$ are frozen at $E_0 = 0.8\,\text{keV}$ and $\Gamma = 2.0$ or 1.8 or 1.6, respectively. Such values are consistent with the interpretation of a non-thermal emission originating from IC off the UV stellar radiation field (see below). These fits include all EPIC detectors (pn, MOS1, MOS2). From the best-fit model we find that the contribution of the non-thermal flux to the energy-integrated source flux in the 0.3-10 keV band is as large as ∼30%. We present the results of the best-fit in Fig. 1.
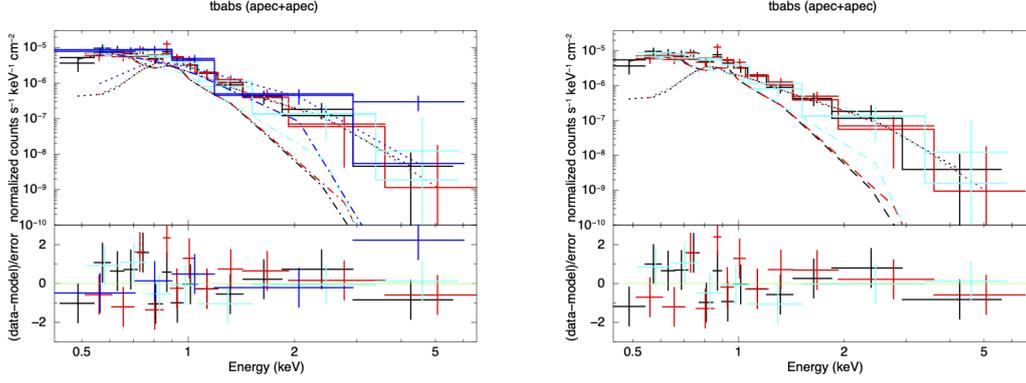
Figure 2: Fit of all the low-flux pn observations shown in the colours black, red, cyan, and blue for OBSIDs 0723540301, 0723540401, 0603740901 and 0552410401, respectively. Left: the time-integrated X-ray spectrum, along with the best-fit model of two thermal absorbed APEC components (dashed-dotted line and dotted line) in the top panel. Fit residuals in terms of sigma with error bars of size 1σ in the bottom panel. Right: same as the left panel but excluding OBSID 0552410401 (blue datapoints).

Low-flux spectrum. In the left panel of Fig.2 we show the low-flux spectrum for all pn observations in different colours. The observation 0552410401 (blue datapoints) appears to show a harder spectrum based on the single data point above 3 keV. The observation 0552410401 is likely not to belong with the low-flux observations, since it shows harder spectrum and higher flux comparable to the high-flux observation. For that reason we performed separate spectral fits including and not including observation 0552410401. The best-fit model (see Fig.2) for both cases (including OBSID 0552410401: $\chi_\nu^2 = 1.12$, and excluding OBSID 0552410401: $\chi_\nu^2 = 1.07$) is given by a two-component thermal plasma model (last two rows of Table 1).

The combined flux-spectrum analysis leads to conclude that a non-thermal component, although not completely suppressed in the transition between the high- and low-flux state, is strongly reduced. A non-thermal contribution might harden the low-flux spectrum via OBSID 0552410401. However, since it contributes only one datapoint (∼ 5 keV) with relative large error in energy, its statistical significance does not allow to firmly conclude that in the low-flux state the high-energy electron population has completely cooled.

Table 1: Best-fit parameters from spectral fitting of the high-flux and low-flux observations

Model	kT_1 keV	$norm_{kT_1}$ $\times 10^{-4}$	kT_2 keV	$norm_{kT_2}$ $\times 10^{-5}$	$norm_\Gamma$ $\times 10^4$	χ^2 (dof)	χ^2_ν
			High-flux				
tb×(a+a)	0.11 ± 0.04	> 35.0	$0.57^{+0.74}_{-0.27}$	$2.4^{+13.6}_{-1.2}$	-	15.0 (19)	0.79
tb×(b+a) (Γ=2.0)	0.17 ± 0.03	$8.7^{+17.6}_{-5.4}$	-	-	1.2 ± 0.6	25.5 (20)	1.27
tb×(b+a) (Γ=1.8)	0.17 ± 0.03	$8.9^{+16.4}_{-5.4}$	-	-	0.9 ± 0.5	25.8 (20)	1.29
tb×(b+a) (Γ=1.6)	0.17 ± 0.03	$8.9^{+15.2}_{-5.5}$	-	-	0.6 ± 0.4	26.4 (20)	1.32
			Low-flux				
tb×(a+a)(incl.)	$0.15^{+0.10}_{-0.06}$	> 2.3	$0.62^{+0.85}_{-0.23}$	$0.6^{+3.1}_{-0.2}$	-	33.58 (30)	1.12
tb×(a+a)(excl.)	$0.14^{+0.09}_{-0.06}$	> 2.4	$0.59^{+0.75}_{-0.22}$	$0.7^{+2.3}_{-0.4}$	-	28.0 (26)	1.07

The normalisation of the APEC component is in units of $\frac{10^{-14}}{4\pi D^2} \int n_e n_H dV$ where n_e and n_H are the electron and hydrogen densities integrated over the volume V of the emitting region and D is the distance to the source in cm. The normalisation of the power-law is in units of photons $keV^{-1} cm^{-2} s^{-1}$ at 1 keV. Here "tb" stands for *tbabs*, "$b+a$" for *bknpower + apec*, "$a+a$" for *apec + apec* and "incl." ("excl") for include (exclude) observation 0552410401.

3. Scenario for the non-thermal emission at pulsation-driven shocks

We compared the time scale of electron acceleration at the pulsation-driven shocks with the time scale of the radiative cooling and the non-thermal energy loss processes relevant to relativistic electrons (Inverse Compton, synchrotron, bremsstrahlung, Coulomb losses) under the constraint that these processes deplete the high-energy electron population on a time scale shorter than the pulsation period t_p.

Cepheids exhibit two-component X-ray emission with shock waves being responsible for the phase-dependent variable emission (phases 0.2–0.6) and with a separate mechanism being the dominant source of emission for the "quiescent" phases, as concluded by [6]. In this scenario, the shock heating acts on this preexisting hot plasma only in locally more rarefied wind regions.

We have introduced the scenario [5] shown in Fig.3 of a stellar pulse that is slowed down by the inhomogeneities in the circumstellar medium; other regions of the pulse unimpeded by overdensities expand and steepen into a travelling shock that heat/ionizes the medium. These latter regions of mostly ionized coronal plasma are subsequently crossed by shock driven by the continuing stellar pulsation.

4. Electron acceleration at pulsation-driven shocks

Generally, a higher acceleration rate at non-relativistic shocks is realized by a higher shock speed, a stronger magnetic field B or a magnetically oblique shock [7, 8]. For the sake of simplicity we apply here the linear version of diffusive shock acceleration (DSA) model to determine the
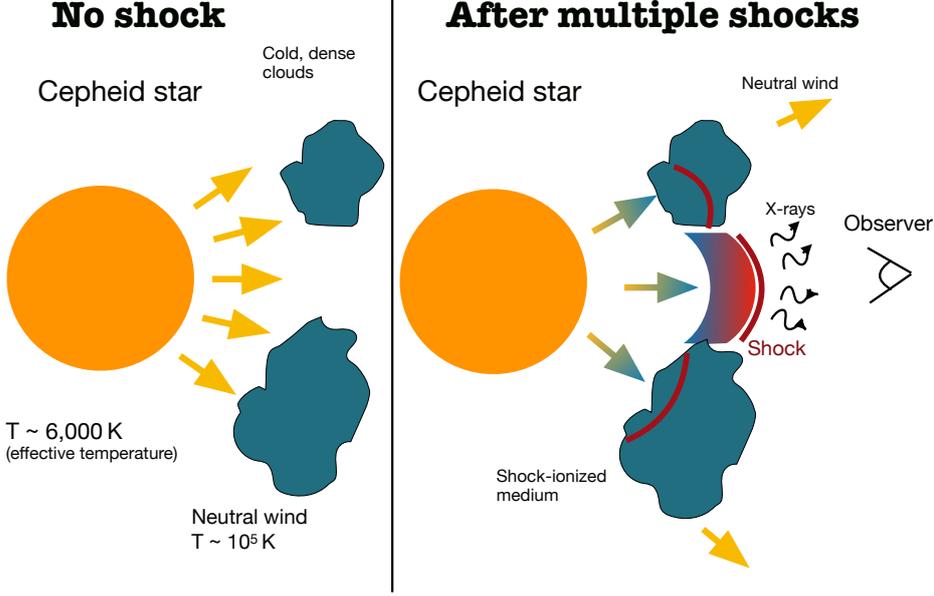
Figure 3: Cartoon illustration of the pulsation-driven shocks propagating into the pre-ionized circumstellar medium.

electron acceleration time scale t_{acc} [8]. For an electron of Lorentz factor γ at a shock moving with speed C_r in the stellar wind frame with an embedded magnetic field $B = |\mathbf{B}|$, t_{acc} can be approximated as [9, 10]

$$t_{acc}(\gamma) \simeq 1.83 \frac{3r^2}{r-1} \frac{D_0(\gamma)}{C_r^2} = 2.4 \times 10^{-4} \mathrm{d} \frac{r^2 k_0}{r-1} \frac{0.01G}{B(3R_\star)} \left(\frac{200km/s}{C_r(R)}\right)^2 \frac{\gamma^2-1}{\gamma} \left(\frac{R}{3R_\star}\right)^3 \quad (1)$$

where r is the density compression at the shock, $D_0(\gamma)$ is the spatial diffusion coefficient for an isotropic upstream turbulence, and $k_0 = D_0/D_B$, assumed to be equal upstream and downstream [9], where D_B is the Bohm diffusion coefficient at the electron Lorentz factor γ. Due to the dipole-like scaling of the magnetic field with the astrocentric distance, i.e., $B \simeq R^{-3}$, the acceleration rate declines rapidly outward from the star, thereby constraining an X-ray emission on a scales shorter than the pulsation period $t_p \sim 5$ days to region very close to the star ($R < 10 R_\star$).

As for the turbulence effect in the shocked region, t_{acc} depends on the geometry of the upstream magnetic field $\mathbf{B}$, i.e., if $\mathbf{B}$ is parallel or perpendicular to the shock normal (see Fig.4). For weak turbulence (far from Bohm regime), it holds that $k_0 \gg 1$ ($k_0 \ll 1$) for shocks in quasi-parallel (or quasi-perpendicular) geometry [e.g., 11]; for strong turbulence (Bohm regime), the total (average + turbulent) magnetic field is nearly isotropic ($k_0 \simeq 1$, blue curve in Fig.4). For a quasi-perpendicular shock the acceleration rate has been long known to be higher [7, 12]. A 100-fold amplification of the magnetic field via turbulent dynamo [13] at the shock propagating through density inhomogeneities in the stellar corona [13] would be required for the synchrotron emission to dominate over the IC; however, such amplification is unlikely for the expected low Mach number.
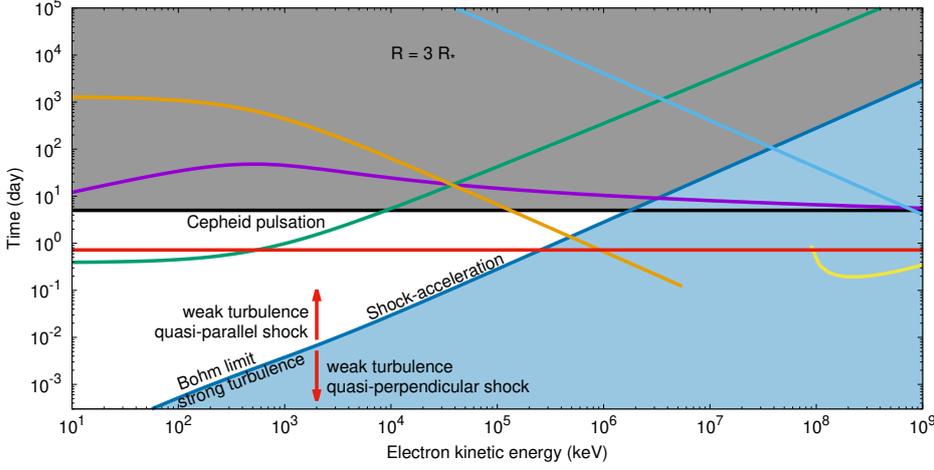
Figure 4: For energetic electrons accelerated at a shock ($r = 4$) travelling through the stellar corona, the time scales for the non-thermal energy losses (bremsstrahlung, IC t_{IC}^T in Thomson and Klein-Nishima regimes), Coulomb, synchrotron), non-radiative shock acceleration t_{acc} (in blue, Bohm regime, or strong magnetic turbulence, i.e., $k_0 = 1$) and thermal radiative cooling t_{rad} are compared with the estimated δ Cep pulsation period t_p (black horizontal line). The shaded blue (blank) area below (above) the blue curve corresponds to the case $k_0 < 1$ ($k_0 > 1$), i.e., weak turbulence at quasi-perpendicular (quasi-parallel) magnetic obliquity. The grey shaded area ($t > t_p$) is ruled out by X-ray observations. Here we used shock speed $C_r = 200$ km/s [6], $n_i(3\,R_\star) = 10^9$ cm^{-3}, $n_H(3\,R_\star) = 10^9$ cm^{-3} and $B(3\,R_\star) = 0.01$ G.

5. Energy losses via Inverse Compton Scattering off the UV stellar background

We proposed [5] that the non-thermal enhanced X-ray emission in $\delta-$Cep originates from UV ($\sim 1-100$ eV) stellar wind photons upscattered into X-ray band by the IC over the shock-accelerated electrons, as proposed by [3] for OB supergiants. The target UV photon population within the photosphere/corona is assumed to be isotropic in the frame of the plasma flowing downstream of the shock, i.e., Doppler effect is negligible for a shock speed $C_r \simeq 200$ km/s. The population of shock-accelerated electrons is also isotropic in the plasma frame at that shock speed.

In the Thomson limit (assuming 5 eV initial photon UV energy), the IC loss time scale at distance R from the stellar surface is

$$t_{IC}^T(\gamma) = \frac{1.3 \times 10^3 \, \mathrm{d}}{\gamma} \left(\frac{6,000 \, K}{T_\star} \right)^4 \left(\frac{R}{3R_\star} \right)^2 . \tag{2}$$

where we have used for the δ Cep stellar surface temperature $T_\star \sim 6,000$ K and the factor $(R/R_\star)^2$ accounts for the scaling of the UV photon energy density integrated over all frequencies (see the orange curve in Fig.4 for $t_{IC}^T(\gamma)$). This curve intersects t_{acc} and t_p (black line) at the smallest energy ($\sim$GeV) making it the most efficient loss process.

6. IC Photon energy spectrum through the stellar corona

By approximating the differential electron spectrum $dN/d\gamma$ as a power law, i.e., $dN/d\gamma = C\gamma^{-\delta}$ with a normalization constant C, we calculate the observed photon spectrum by folding $dN/d\gamma$ with the single electron IC power off the photon blackbody distribution in the stellar wind [5].

The UV radiation field scattered photons and the energetic electrons are assumed to be isotropically distributed; if isotropy of electrons is not altered to the lowest order by the slow wind motion, the radially expanding wind UV field has to be isotropic [3]. In the Thomson scattering limit, the IC scattered power per unit of volume and energy can be written as [eq. 7.31, 14]

$$\frac{dE}{dV dt\, d\epsilon_1} = \frac{3\pi\sigma_T C}{h^3 c^2}\bar{F}(\delta)(k_B T)^{(\delta+5)/2}E^{-\frac{\delta-1}{2}},$$

(3)

where σ_T is the Thomson cross-section, h the Planck constant and $\bar{F}(\delta) \simeq 1$. Due to the scaling of the wind temperature $T(R) = T(R_\star)(R_\star/R)^{1/2}$, the photon flux per unit of energy emitted during the shock expansion between two radii R_i and R_f can be recast as

$$
\begin{aligned}
F(E; R_f, R_i) &= \frac{1}{E}\int_{R_i}^{R_f}\frac{dE}{dV dt\, d\epsilon_1}\left(\frac{R}{d}\right)^2 dR = \frac{3\pi\sigma_T C}{h^3 c^2}\bar{F}(\delta)(k_B T)^{\frac{\delta+5}{2}}\frac{R_\star^3}{d^2}\frac{4}{7-\delta}\left(\frac{R_f}{R_i}\right)^{(7-\delta)/4}E^{-\frac{\delta+1}{2}}\\
&\propto E^{-\frac{\delta+1}{2}}\quad[\frac{\text{photons}}{\text{cm}^2\,\text{s}\,\text{keV}}]
\end{aligned}
$$

(4)

where d is the Cepheid-Earth distance.

Thus, for a flux per unit energy $F(E; R_f, R_i)$ fitted by the non-thermal power law component with index Γ (see Sect.2), the power law index of the electrons energy distribution is $\delta = 2(\Gamma-1)+1$ [14]. In table 2 a value $\Gamma \sim 1.6$ ($\delta = 2.2$) leads to $\chi^2 = 1.32$. The linear DSA links the electron spectral index of the phase space distribution function s ($s = \delta + 2$) with the assumed energy-independent shock density compression $r = s/(s-3) \sim 2.5$ (and $r = 3.5$ for $\delta = 2.2$). For radiative shocks the density compression depends on the electron energy because the thickness of the downstream cooling region is greater for higher electron energy [e.g., 15]. This effect is neglected herein due to the near-balance of the cooling with the IC time scale shown in Fig. 4.

7. Conclusion

We have outlined the recent work [5] on 1) an updated spectral fit of the thermal/non-thermal components of the enhanced X-ray emission observed by XMM-Newton in δ Cep [1] and 2) a scenario of pulsation-driven shocks travelling through pre-ionization stellar corona and efficiently accelerating electrons to multi-GeV. Our analytic analysis, combined with previous hydrodynamic simulations [6], suggests that IC over the UV background stellar field dominates the energy losses. The lack of periodic radio counterpart associated with stellar pulsation [16] supports this scenario.

References

[1] S.G. Engle, E.F. Guinan, G.M. Harper, M. Cuntz, N. Remage Evans, H.R. Neilson et al., *The Secret Lives of Cepheids: δ Cep—The Prototype of a New Class of Pulsating X-Ray Variable Stars*, **838** (2017) 67 [1702.06560].

[2] L.B. Lucy, *X-ray emission from the winds of hot stars. II.*, **255** (1982) 286.

[3] W. Chen and R.L. White, *Nonthermal X-Ray Emission from Winds of OB Supergiants*, **366** (1991) 512.

[4] W. Chen and R.L. White, *Inverse-Compton Gamma-Ray Emission from Chaotic, Early-Type Stellar Winds and Its Detectability by Gamma Ray Observatory*, **381** (1991) L63.

[5] F. Fraschetti, K. Anastasopoulou, J.J. Drake and N.R. Evans, *Nonthermal X-Rays from Pulsation-driven Shocks in Cepheids*, **944** (2023) 62 [2212.08150].

[6] S.-P. Moschou, N. Vlahakis, J.J. Drake, N.R. Evans, H.R. Neilson, J.A. Guzik et al., *Phase-modulated X-Ray Emission from Cepheids due to Pulsation-driven Shocks*, **900** (2020) 157 [2007.11545].

[7] J.R. Jokipii, *Particle drift, diffusion, and acceleration at shocks*, **255** (1982) 716.

[8] L.O. Drury, *An introduction to the theory of diffusive shock acceleration of energetic particles in tenuous plasmas*, *Reports on Progress in Physics* **46** (1983) 973.

[9] E. Parizot, A. Marcowith, J. Ballet and Y.A. Gallant, *Observational constraints on energetic particle diffusion in young supernovae remnants: amplified magnetic field and maximum energy*, **453** (2006) 387 [astro-ph/0603723].

[10] F. Fraschetti, S. Katsuda, T. Sato, J.R. Jokipii and J. Giacalone, *Vortical Amplification of the Magnetic Field at an Inward Shock of Supernova Remnant Cassiopeia A*, *Physical Review Letters* **120** (2018) 251101 [1805.05951].

[11] F. Fraschetti and J. Giacalone, *Early-time Velocity Autocorrelation for Charged Particles Diffusion and Drift in Static Magnetic Turbulence*, **755** (2012) 114 [1206.6494].

[12] J.R. Jokipii, *Rate of energy gain and maximum energy in diffusive shock acceleration*, **313** (1987) 842.

[13] F. Fraschetti, *Turbulent Amplification of a Magnetic Field Driven by the Dynamo Effect at Rippled Shocks*, **770** (2013) 84 [1304.4956].

[14] G.B. Rybicki and A.P. Lightman, *Radiative Processes in Astrophysics* (1986).

[15] J.H. Krolik and J.C. Raymond, *Radiation pressure-driven shocks in winds from hot stars*, **298** (1985) 660.

[16] L.D. Matthews, N.R. Evans and M.P. Rupen, *First Detection of Radio Emission Associated with a Classical Cepheid*, **165** (2023) 92 [2301.04666].